Defects controlling electrical and optical properties of electrodeposited Bi doped Cu_2O

Iuri S. Brandt, Milton A. Tumelero, Cesar A. Martins, Cristiani C. Plá Cid, Ricardo Faccio, and André A. Pasa

Citation: Journal of Applied Physics **123**, 161412 (2018); doi: 10.1063/1.5007052
View online: https://doi.org/10.1063/1.5007052
View Table of Contents: http://aip.scitation.org/toc/jap/123/16
Published by the American Institute of Physics

Defects controlling electrical and optical properties of electrodeposited Bi doped Cu_2O

Iuri S. Brandt,[1,2] Milton A. Tumelero,[1,3] Cesar A. Martins,[1] Cristiani C. Plá Cid,[1] Ricardo Faccio,[4] and André A. Pasa[1]

[1]*Laboratório de Filmes Finos e Superfícies, Departamento de Física, Universidade Federal de Santa Catarina, Florianópolis, SC 88040-900, Brazil*
[2]*Programa de Pós-Graduação em Ciência e Engenharia de Materiais, Universidade Federal de Santa Catarina, Florianópolis 88040-900, Brazil*
[3]*Instituto de Física, Universidade Federal do Rio Grande do Sul, Porto Alegre 91501-970, Brazil*
[4]*Centro NanoMat/Cryssmat Lab, DETEMA, Facultad de Química, Universidad de la República, Montevideo, Uruguay*

(Received 29 September 2017; accepted 18 February 2018; published online 14 March 2018)

Doping leading to low electrical resistivity in electrodeposited thin films of Cu_2O is a straightforward requirement for the construction of efficient electronic and energy devices. Here, Bi (7 at. %) doped Cu_2O layers were deposited electrochemically onto Si(100) single-crystal substrates from aqueous solutions containing bismuth nitrate and cupric sulfate. X-ray photoelectron spectroscopy shows that Bi ions in a Cu_2O lattice have an oxidation valence of 3+ and glancing angle X-ray diffraction measurements indicated no presence of secondary phases. The reduction in the electrical resistivity from undoped to Bi-doped Cu_2O is of 4 and 2 orders of magnitude for electrical measurements at 230 and 300 K, respectively. From variations in the lattice parameter and the refractive index, the electrical resistivity decrease is addressed to an increase in the density of Cu vacancies. Density functional theory (DFT) calculations supported the experimental findings. The DFT results showed that in a 6% Bi doped Cu_2O cell, the formation of Cu vacancies is more favorable than in an undoped Cu_2O one. Moreover, from DFT data was observed that there is an increase (decrease) of the Cu_2O band gap (activation energy) for 6% Bi doping, which is consistent with the experimental results. *Published by AIP Publishing*. https://doi.org/10.1063/1.5007052

I. INTRODUCTION

Cuprous oxide (Cu_2O) is a semiconductor with a direct band gap of ∼2.17 eV at 4.2 K (Ref. 1) and natural hole conduction character.[2] It has attracted attention as a low-cost material for application in photovoltaic water splitting cells,[3] transistors,[4] catalysis,[5] photocatalysis,[6] and solar cells.[7] Recently, Cu_2O was also considered as a promising photoconductive switching material since it presented a switching ratio of 3.25 and a response time of 0.45 s.[8] For the production of thin films of Cu_2O, a broad range of techniques have been used, e.g., pulsed laser deposition,[9] magnetron sputtering,[10] copper oxidation,[7] radical oxidation,[11] and electrodeposition.[12,13] In particular, Cu_2O grown by electrodeposition is very attractive, since it involves low instrumental and materials cost, and is efficient for producing large area films.[14–16] Electrodeposition also easily enables the modification of Cu_2O properties that are dependent on the pH of the electrolyte,[13,17] such as the crystallographic orientation, the morphology and the refractive index.

The electrical resistivity of electrodeposited Cu_2O films can reach too high values such as 10^8 Ω cm (Refs. 18–22) that are detrimental to developing semiconductor devices with high efficiency.[23] A low fill factor (FF) has been obtained in electrodeposited p-n homojunction Cu_2O solar cells,[21,24–27] and the main cause is the high series resistance of the cell.

Doping processes are used in materials engineering with the aim to increase the density of majority carriers, and consequently decrease the electrical resistivity of the semiconductors.[28] Through Cl doping, an expressive reduction of about 5 orders of magnitude in electrical resistivity has been obtained for electrodeposited Cu_2O films.[29] Nevertheless, this doping process actually gives Cu_2O n-type character.[29,30] For Cu_2O p-n homojunction solar cells, Cl doping can be quite useful, but it still remains a necessity for a dopant that could effectively reduce the Cu_2O resistivity, but retaining its p-type character. For electrodeposited Cu_2O films, a decrease in the electrical resistivity by a factor of 3 by doping with 0.3 at. % Mn was measured.[31] However, it was not elucidated if that doping process induces acceptor or donor states inside of the Cu_2O band gap.

Si- and Ge-doped Cu_2O thin films grown by sputter deposition showed electrically active acceptors in the band gap and a reduction of electrical resistivity by one order of magnitude.[32,33] A decrease of three orders of magnitude in electrical resistivity was measured for sputter-deposited Cu_2O films doped with N, preserving the p-type character.[34] The reduction of Cu_2O electrical resistivity and enhancement of carrier concentration were also attained by N doping of Cu_2O grown via radical oxidation.[35]

Motivated by the technological interest in electrodeposited p-type Cu_2O films with low electrical resistivity and encouraged by the results found for Cu_2O doped with Ge, Si, and N, this work aimed to dope electrodeposited p-type Cu_2O thin films looking for a decrease of the electrical resistivity maintaining the p-type character. It will be shown that by doping with Bi, the Cu_2O electrical resistivity is reduced

and the reduction can be associated with the enhancement of the density of Cu vacancies (V_{Cu}) in the lattice, as concluded from structural, optical and electrical characterization. All experimental results are supported by first principles calculations.

II. METHODS

A. Experimental

Cu_2O electrodeposition was carried out in a conventional three electrode cell connected to a potentiostat Autolab PGSTAT30. As the working electrode, n-type (100) silicon (n-Si) wafers with resistivity in the range of 6–9 Ω cm were employed. The counter-electrode was a Pt foil and the reference electrode a Saturated Calomel Electrode (SCE). Before Cu_2O electrodeposition, the silicon substrates were immersed in a 5% HF solution for 30 s to remove the native oxide from the Si surface. The electrolyte for the electrodeposition of undoped Cu_2O thin films was prepared from analytical grade reagents, and contained 0.4 M $CuSO_4$ and 3.0 M lactic acid dissolved in deionized water. The electrolyte pH was adjusted to 9.0 by adding 5.0 M sodium hydroxide. For the growth of Bi-doped Cu_2O samples, 15 mM $Bi(NO_3)_3$ was added to this electrolyte. All Cu_2O films were grown by potentiostatic deposition at room temperature (RT), with three different applied potentials of −0.375, −0.400, and −0.425 V *vs*. SCE.

The electrical properties of Cu_2O were investigated by current *vs*. voltage measurements in the temperature interval between 230 and 300 K. In order to obtain reproducible electrical contacts, several circular areas of 0.5 mm^2 of Au (forming an array of contacts) were e-beam evaporated at pressures of 1×10^{-7} Torr on top of the Cu_2O surface. The Au/Cu_2O junction forms ohmic contacts.[30] The Au/Cu_2O/n-Si structures were used to ensure p-type behavior and for the evaluation of the resistivity of Cu_2O layers. The interface Cu_2O/n-Si forms a p-n junction, as will be described below. Further characterization was performed by X-ray Diffraction (XRD) with a PANalytical equipment, model X'PERT with $CuK_{\alpha 1}$ radiation; Atomic Force Microscopy (AFM) with a system from Molecular Imaging, model PicoScan; Transmission Electron Microscopy (TEM) with a JEOL microscope model JEM-2100; UV/Vis/NIR reflectance spectroscopy with a Perkin Elmer spectrophotometer, model Lambda 750 with an integration sphere of 60 mm; X-ray Photoelectron Spectroscopy (XPS), with a Thermo Fisher Scientific ESCALAB 250Xi with monochromatic Al Kα X-rays and a spot size of 650 μm, and Energy Dispersive Spectroscopy (EDS), with a Scanning Electron Microscope (JEOL JSM-6390LV).

B. Computational

Density functional theory (DFT) based calculations were performed in the Vienna Ab initio Simulation Package (VASP 5.3)[36] by using GGA (Gradient-corrected approximation) + U (Perdew-Burke-Ernzerhof parameterization[37]) and hybrid functionals (HSE06 parametrization[38]) for structural relaxation and electronic structure calculation, respectively. The core-valence interaction was described through a Projected Augmented Wave Method,[39] and semicore pseudopotentials were used for Cu and Bi representation. The crystalline structure was simulated within the supercell approach, in which a $2 \times 2 \times 2$ cell containing 48 atoms was employed with a fixed lattice parameter of 4.2859 Å. The onset Hubbard energy, U = 5.2 eV, was chosen from Ref. 40 and used to obtain the optimized lattice parameter and also for supercell relaxation. The wavefunction basis energy cutoff was 400 eV and the k-point sampling was a $4 \times 4 \times 4$ mesh for ionic relaxation within PBE (Perdew-Burke-Ernzerhof) parameterization and a gamma point only for electronic calculation within HSE06 parametrization and spin-orbit coupling.

The formation energy of dopant sites ΔH_f is calculated using the following equation:[40]

$$\Delta H_f = E(D,q) - E_0^{bulk} + \sum n_i(E_i + \mu_i) + q\varepsilon_F, \quad (1)$$

where $E(D,q)$ is the total energy of a supercell with defect "D" and charge "q," E_0^{bulk} is the total energy of the host supercell, n_i is the number of atoms of element "i" added or removed from the supercell, E_i is the reference energy of element "i," μ_i is the chemical potential of element "i," and ε_F is the Fermi level inside the bandgap. To obtain the reference energies, bulk calculations of Bi (space group $R\bar{3}mH$), Cu (space group $Fm\bar{3}m$) and O_2 were performed.

The pH equilibrium conditions were introduced by choosing the value of μ_i resulting from the global constraint over the host enthalpy, given by the expression

$$\Delta H_{Cu_2O} \geq 2\mu_{Cu} + \mu_O, \quad (2)$$

where μ_{Cu} and μ_O are the chemical potentials for copper and oxygen, respectively, and ΔH_{Cu_2O} is the enthalpy of formation for Cu_2O of about −1.55 eV, the same value as found in Ref. 40. For pH simulation, we introduce a new constraint expression,[22] given by

$$\Delta H_{H_2O} \geq \mu_{OH^-} + \mu_{H^+}, \quad (3)$$

where ΔH_{H_2O} is the water enthalpy with the calculated value of −2.597 eV, close to the one found in Ref. 41 and μ_{OH^-} is the chemical potential of hydroxyl, assumed to be 0 in a basic medium, and μ_{H^+} is the chemical potential of hydrogen ions, assumed to be zero in acid medium. In order to introduce Bi dopants, another equilibrium condition is taken, that is an equilibrium with the bismuth oxide phase Bi_2O_3, given by the following expression:

$$\Delta H_{Bi_2O_3} \geq 2\mu_{Bi} + 3\mu_O, \quad (4)$$

where $\Delta H_{Bi_2O_3} = -6.047$ eV is the enthalpy of Bi_2O_3. Following these conditions, the values for the chemical potential in the basic medium are calculated as

$$\mu_{Cu} = -2.074\,\text{eV}, \quad \mu_O = 2.597\,\text{eV}, \quad \mu_{Bi} = -6.919\,\text{eV}, \quad (5)$$

and also in acid medium as

$$\mu_{Cu} = 0.524\,\text{eV}, \quad \mu_O = -2.597\,\text{eV}, \quad \mu_{Bi} = 0.872\,\text{eV}. \quad (6)$$

All the reference compounds were calculated using GGA + U, with the same Cu onset energy.

III. RESULTS

A. Structural and morphological characterization

The concentration of Bi atoms in doped Cu_2O films was firstly measured by EDS. Figure 1(a) shows the intensities of O, Cu and Bi EDS peaks, which are not dependent on the applied potential for Cu_2O deposition. Consequently, an equal Bi amount of 7 at. % was evaluated from films electrodeposited in the three tested potentials of −0.375, −0.400 and −0.425 V *vs.* SCE. Particle Induced X-ray Emission (PIXE) and X-ray Photoelectron Spectroscopy (XPS) measurements confirmed the value of 7 at. % (results not shown). The oxidation state of the incorporated Bi atoms was investigated through the Bi 4f XPS spectrum, which is shown in Fig. 1(b). The Bi $4f_{5/2}$ and $4f_{7/2}$ peaks are, respectively, located at 164.3 and 159.0 eV. These peak positions are assigned to Bi^{3+} ions,[42] and were found out by fitting the experimental curve by Gaussian (70%)-Lorentzian (30%) profiles. This result, in principle, indicates the non-presence of metallic Bi, whose 4f binding energies are 162.4 and 157.1 eV.[42]

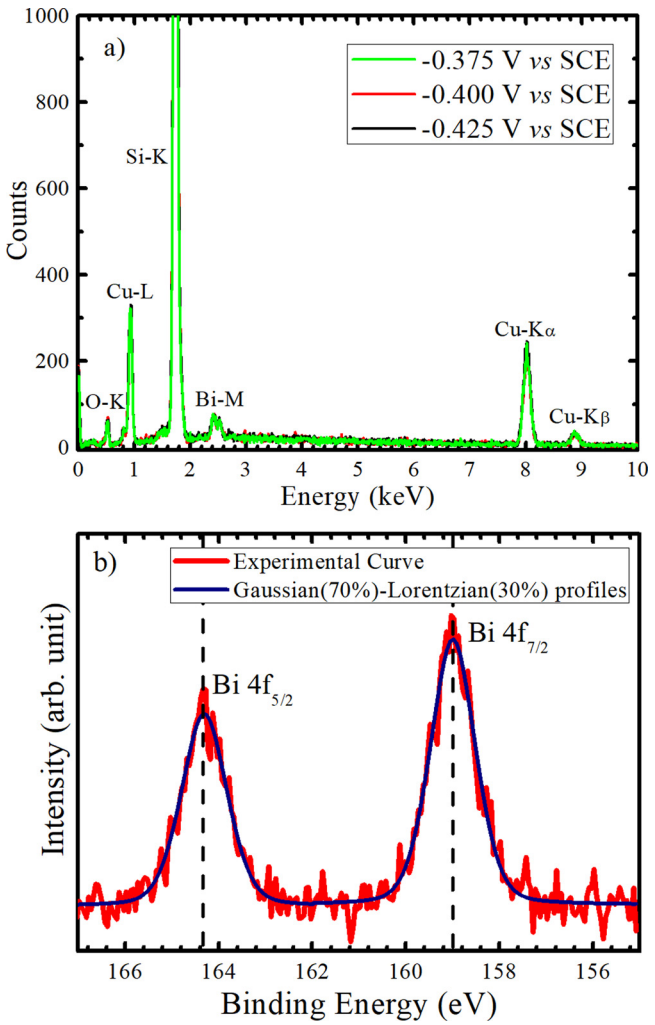

FIG. 1. (a) EDS spectra of Cu_2O films electrodeposited at −0.375, −0.400, and −0.425 V *vs.* SCE. From these spectra was calculated a Bi concentration of 7 at. % for the three Cu_2O samples. (b) Bi 4f XPS spectral characteristic of all deposited Bi doped Cu_2O layers independent of the applied potential. The peak positions are as expected for Bi^{3+} ions.

XRD measurements in the glancing angle configuration ($\omega = 1.5°$) of Bi-doped Cu_2O films were performed to check for the existence of secondary phases related to Bi^{3+} ions. As shown in Figs. 2(a)–2(c), independent of the deposition potential, no Bi phases were observed, i.e., only peaks from Cu_2O crystals are present.[43] For Bi-doped samples, the Cu_2O lattice parameter calculated for all peaks present in the diffractogram showed the same value of 4.22 Å and a full-width at half maximum (FWHM) of 0.4°. The glancing angle XRD pattern of an undoped Cu_2O sample electrodeposited at −0.400 V *vs.* SCE is displayed in Fig. 2(d), and the lattice parameter found in this case is 4.27 Å, which is the value expected for the strain-free Cu_2O lattice.[43] The observed smaller lattice parameter for doped films is probably related to the incorporation of Bi ions into the Cu_2O lattice, which could induce the formation of copper vacancies (V_{Cu}).[44] From Bragg-Brentano XRD measurements, whose diffractograms are not shown, the preferential growth direction of the Cu_2O layers was checked. Table I displays the percentage of Cu_2O crystallites growing in the [100] direction. These values were obtained following the procedure adopted in Ref. 17 and show that less negative electrodeposition potential favors the [100] growth direction. This behavior is in agreement with the results of Ref. 45.

The structural characterization of Bi doped Cu_2O layers was also carried out by means of Transmission Electron Microscopy (TEM), and it was observed that the film shows a columnar growth. One of the observed columns is presented in Fig. 3(a), showing that the width becomes larger as the film grows, as previously observed for Cu_2O growth on

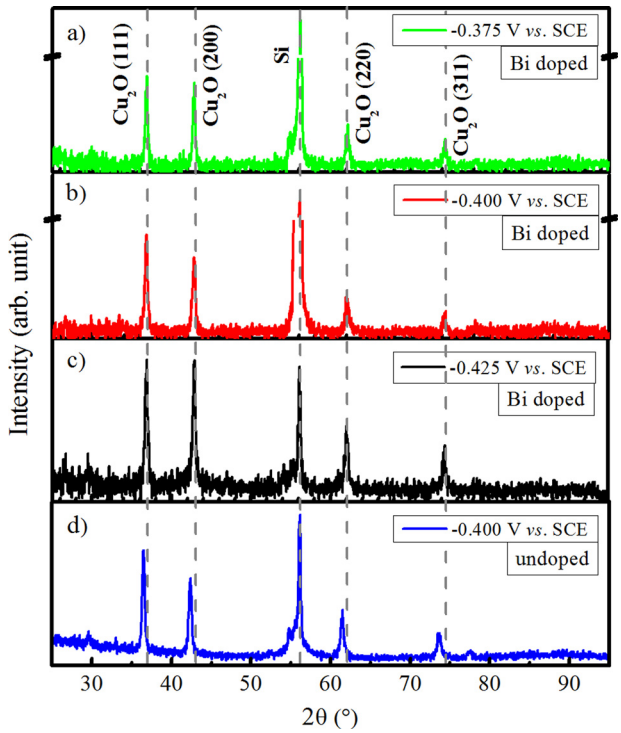

FIG. 2. Glancing angle ($\omega = 1.5°$) XRD of Bi doped Cu_2O films grown under an applied potential of (a) −0.375, (b) −0.400, and (c) −0.425 V *vs.* SCE, and (d) of an undoped Cu_2O film electrodeposited at −0.400 V *vs.* SCE. No Bi phases are found and a shift in Cu_2O XRD peaks is produced by Bi^{3+} doping.

TABLE I. Percentage of Cu_2O crystallites growing in the [100] direction calculated from XRD patterns obtained in Bragg-Brentano mode. Clearly, less negative electrodeposition potentials favor the [100] growth.

Bi doped samples	Applied deposition potential vs. SCE		
Growth direction [100]	−0.425 V 60%	−0.400 V 65%	−0.375 V 69%

Si and Ni substrates.[46] A high-resolution image of this column is shown in Fig. 3(b). The well-defined Cu_2O atomic planes are an indication that, despite the weak texture of the whole film, each column presents good crystalline quality in agreement with the small value of 0.4° for the FWHM of the XRD peaks. TEM high-resolution images of different regions showed no evidence about the formation of Bi phases, also in agreement with XRD measurements. The SiO_2 layer at the Cu_2O/Si interface was previously observed in the literature.[47]

Figures 4(a)–4(c) show AFM images recorded for Cu_2O films with 250 nm of thickness electrodeposited under the three potential conditions. As a general trend, all films present granular morphology, although the sample deposited at −0.375 V *vs.* SCE shows grains with a larger size. The surface roughness, root-mean-square height deviation, was directly calculated using the software PicoScan 5.3 from Molecular Imaging. As observed in Fig. 4(d), the surface roughness increases as a function of the film thickness and is higher for films electrodeposited at −0.375 V *vs.* SCE. The larger grain size and the higher surface roughness observed at −0.375 V *vs.* SCE can be understood through the nucleation-growth-collision theory.[48] Cu_2O films grown at −0.425 V and −0.400 V *vs.* SCE present a higher rate of deposition than those at −0.375 V *vs.* SCE; therefore, at these more negative potentials, Cu_2O islands grow faster and sooner will collide with each other. This accelerated growth of islands deposited at more negative potentials ends up limiting the two-dimensional growth, which results in smaller grain size and lower surface roughness.

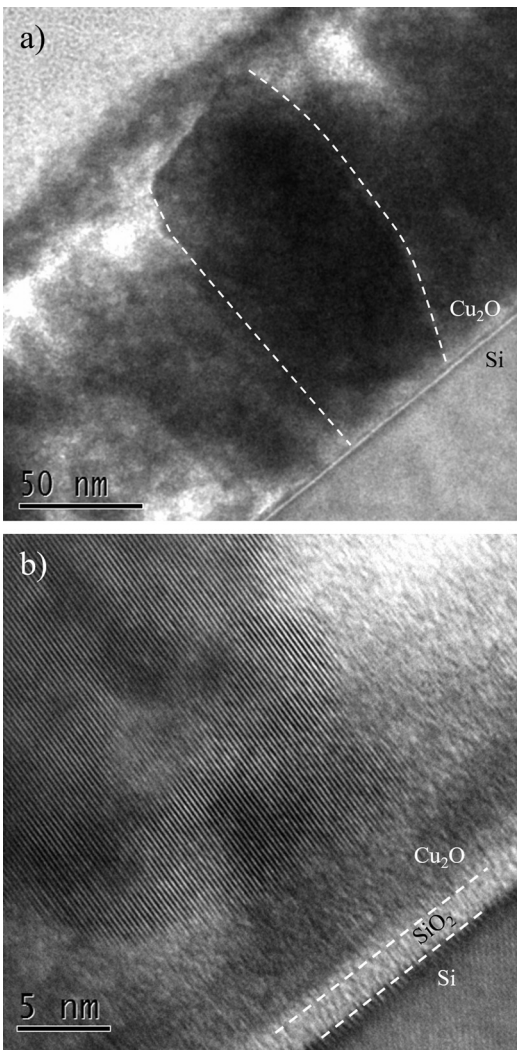

FIG. 3. Cross-section images of the Bi doped Cu_2O film deposited at −0.400 V *vs.* SCE. In (a) is shown a Cu_2O column, delimited by the white dashed line. In (b) is a high resolution TEM image of the column presented in (a).

B. Optical characterization

Figure 5 presents reflectance spectra obtained for undoped and Bi doped Cu_2O films. The oscillatory behavior of the reflectance spectra is due to interference in the Cu_2O films. For wavelengths (λ) lower than ~500 nm, there are no oscillations due to the Cu_2O band gap. Note that the positions in λ for the maxima and the minima of the reflectance spectra strongly depend on doping, and are weakly dependent on the deposition potential. It indicates that Bi doping modifies the Cu_2O band gap and the refractive index, as will be discussed below.

The band gap energy (E_g) and the refractive index of electrodeposited Cu_2O films were obtained from the reflectance measurements following the procedure employed in Ref. 17, and references therein. In Fig. 6(a), E_g is plotted as a function of the deposition potential. For undoped conditions, the mean E_g value is ~2.16 eV and for the doped case, it is ~2.22 eV. Both E_g values are in the range expected for Cu_2O. The enhancement of E_g for Cu_2O doped with Bi can be explained by a decrease in Cu-Cu internetwork interactions.[44,49] The Cu_2O crystal structure constitutes two interpenetrating three-dimensional Cu_2O networks, which are stabilized by Cu-O intranetwork bonds and Cu-Cu internetwork interactions.[50] Theoretical works in the literature show that the attenuation of Cu-Cu internetwork interactions increases the Cu_2O band gap.[44,49] Such Cu-Cu interaction can be suppressed by decreasing the lattice parameter of the interpenetrating Cu_2O networks. As observed from XRD patterns in Fig. 2, Bi doping reduced the Cu_2O lattice parameter. Therefore, this structural modification led to a weaker Cu-Cu interaction, and consequently a higher E_g. Recently, our group has observed the same relationship between E_g and the lattice parameter for undoped Cu_2O films prepared under different deposition conditions[17] and Cu_2O films with different doping levels of Co ions.[22]

Figure 6(b) shows the refractive index as a function of the wavelength for undoped and doped Cu_2O films. The Cu_2O refractive index is weakly dependent on the deposition potential and is significantly affected by doping with Bi. The

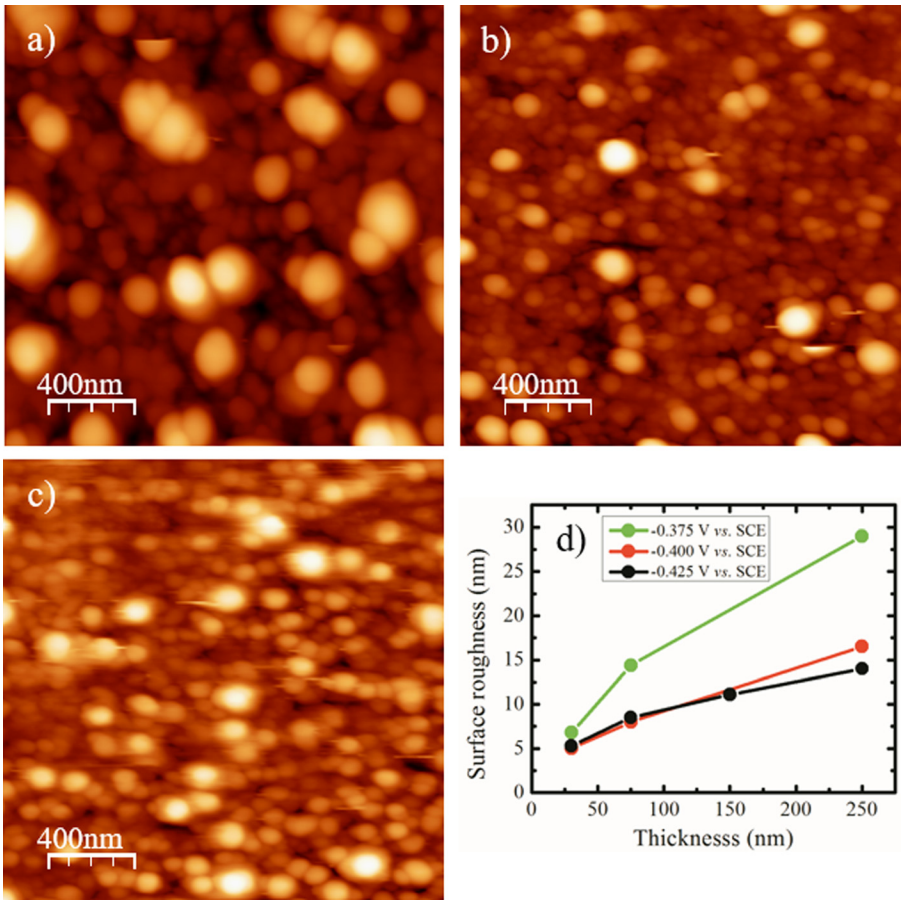

FIG. 4. AFM images of Bi doped Cu_2O films electrodeposited at (a) −0.375, (b) −0.400 and (c) −0.425 V *vs*. SCE. In (d) is displayed the surface roughness calculated from AFM images of doped films with different thicknesses.

noticeable influence of Bi doping on the Cu_2O refractive index is reasonable, since 7% doping is an expressive doping level and is expected to induce appreciable structural distortions and formation of point defects, which are likely to modify the Cu_2O refractive index.[17,22] Meanwhile, despite the deposition potential playing an important role in the film growth dynamics, it is not likely that a variation of only 0.05 V on the deposition potential would lead to structural modifications comparable with the ones induced by 7% Bi doping. However, in order to obtain qualitative information regarding the density of defects in the Cu_2O lattice, we applied the Wemple and DiDomenico (WD) dispersion relationship[51] to the refractive index data.

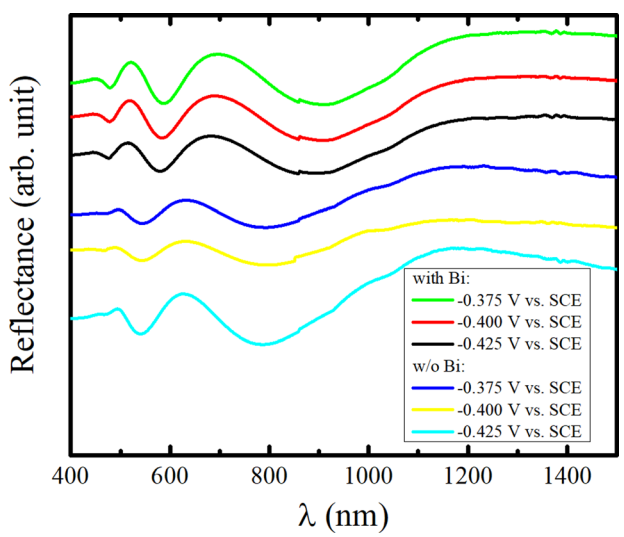

FIG. 5. Optical reflectance spectra of undoped and Bi doped Cu_2O films.

The Wemple and DiDomenico (WD) dispersion relationship[51] is derived from the Sellmeier single-oscillator model. In the WD relationship, the stronger oscillator (electronic transition) is isolated, and the remaining oscillators (electronic transitions) terms are combined. The WD relationship is given by

$$(n^2-1)^{-1} = \frac{E_m}{E_d} - \frac{1}{E_d E_m}(h\nu)^2, \tag{7}$$

where $h\nu$ is the incident radiation energy, E_m is the single-oscillator energy, and E_d is the dispersion energy

$$E_d = \frac{4\pi\hbar^2 N e^2}{m E_m}\sum_k \frac{w_1^2}{w_k^2} f_k, \tag{8}$$

where $\hbar$ is the reduced Planck constant, N is the effective electron density, m is the electron mass, e is the electron charge, w_1 is the frequency associated with the stronger oscillator or transition and f_k is the electric-dipole oscillator strength of a transition at frequency w_k. Crystalline distortions/imperfections, as punctual defects, can affect the N and transition frequency. Therefore, the energy E_d can be useful to look for defects in different crystal systems. Indeed, such information given by E_d has already been used in other works.[17,52,53]

In order to obtain an estimate for E_d, it is helpful to make use of the following empirical relationship, which was

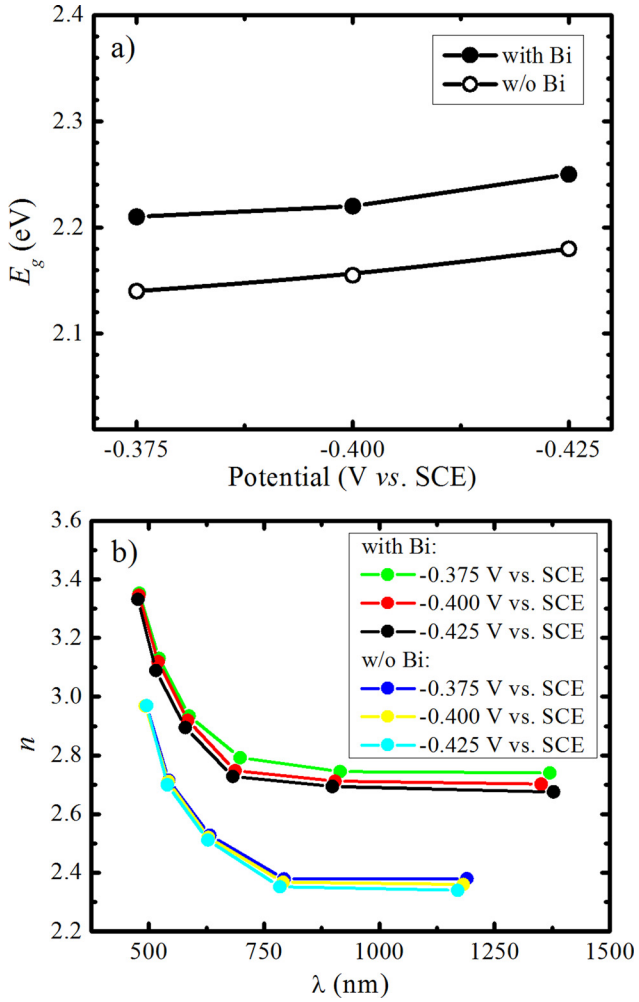

FIG. 6. (a) Band gap energy E_g of undoped and doped Cu_2O films as a function of the applied potential for electrodeposition. (b) Refractive index n as a function of incident wavelength λ of Cu_2O layers with and without Bi^{3+} doping.

proposed by WD for crystals containing a single anion species[51]

$$E_d = \beta.N_e.Z_a.N_c, \tag{9}$$

where N_e is the effective number of valence electrons per anion, N_c is the coordination number of the nearest-neighbor cation, Z_a is the formal anion valency, and the parameter β is bi-valued: $\beta = 0.26 \pm 0.04$ eV for most ionic oxides and $\beta = 0.37 \pm 0.05$ eV for covalent crystals. In the case of Cu_2O crystals, these parameters are: $\beta = 0.26 \pm 0.04$ eV, $N_e = 8$, $N_c = 2$ and $Z_a = 2$, and according to Eq. (9), E_d will be equal to 8.3 ± 1.3 eV.

Figure 7(a) displays $(n^2-1)^{-1}$ *vs.* $(h\nu)^2$ plots for undoped and Bi-doped samples. From the linear region delimited by two vertical discontinuous lines were extracted the energies E_m and E_d of each Cu_2O film. As shown in Fig. 7(b), E_m is about 0.2 eV higher for Bi doped than for undoped Cu_2O films. This higher value is in agreement with the increase of E_g with doping, see Fig. 6(a), since the WD model suggests a direct proportionality between E_m and E_g.[51] In Fig. 7(c), E_d presents values around 13 and 19 eV for undoped and Bi-doped films, respectively. Both E_d

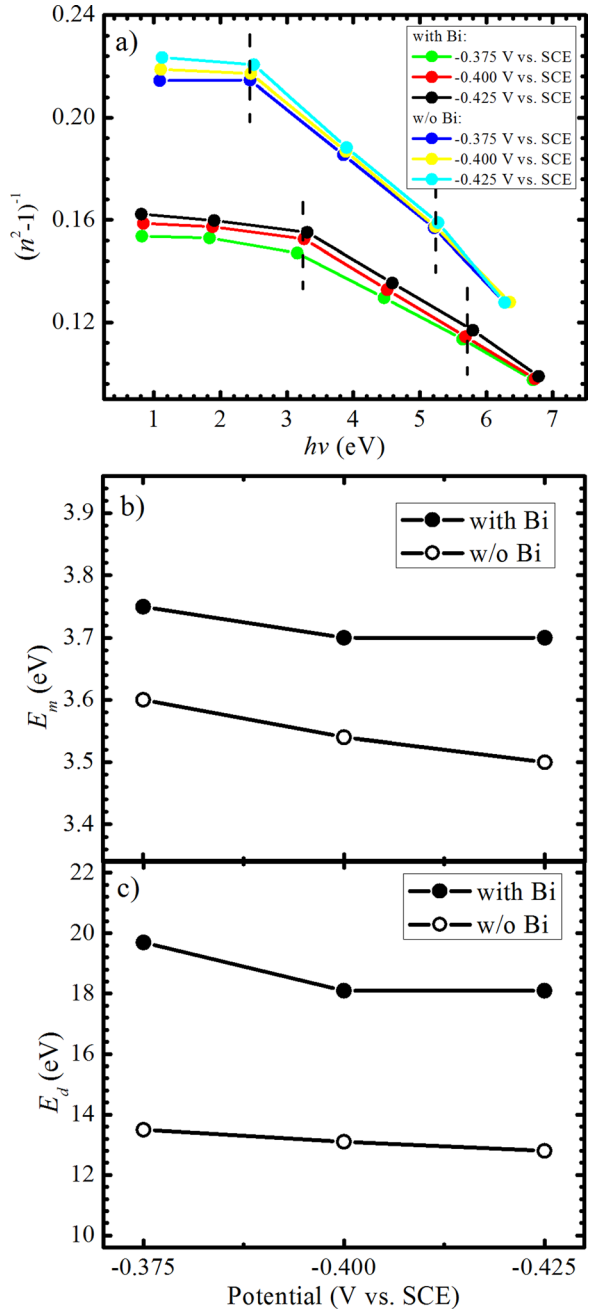

FIG. 7. (a) Dispersion plot following the WD model. The vertical discontinuous lines delimit the linear region for the calculation of E_d and E_m energies. (b) E_d and (c) E_m values against the potential for the electrodeposition of Bi doped and undoped Cu_2O films.

values are far from the nominal value calculated above by Eq. (9) of about 8.3 eV, and the reason could be assigned to distortions in the charge distribution within the Cu_2O lattice caused, e.g., by point defects. As in Cu_2O crystals, V_{Cu} has low formation energy,[54] the value of E_d for the undoped samples is expected to be different from the nominal one calculated for a Cu_2O lattice free of defects. Moreover, since the Cu_2O lattice parameter shrinks for Bi doping, as observed by XRD in Fig. 2, and associated with the formation of V_{Cu} defects, it is reasonable to expect an even higher difference between the nominal value of E_d and the one found for Bi-doped Cu_2O.

C. Electrical characterization

The current-voltage ($I \times V$) curves at RT for the Au/Cu_2O/n-Si structure are presented in Fig. 8(a), and the characteristic behavior of a p-n junction is observed with rectification action for negative voltages applied to the n-type semiconductor. This result is evidence that Bi-doping retains the p-type electrical conductivity of Cu_2O. Bi-doped samples presented a higher direct current, and a dependence of the current with the deposition potential, less negative voltages resulted in higher currents.

In order to find out the Cu_2O electrical resistivity, the region at forward bias in $I \times V$ curves was analyzed following the procedure in Ref. 55. In Fig. 8(b) are presented curves for Cu_2O electrical resistivity as a function of temperature for undoped and Bi doped Cu_2O films. The undoped sample was electrodeposited at pH 10.0 since undoped films grown at pH 9.0 could not be measured.[56] The measured resistivity of about 10^8 Ω cm at RT is usually reported in the literature for electrodeposited Cu_2O.[18–22] However, by doping with Bi, a reduction in resistivity of about 4 orders of magnitude at 230 K and 2 orders of magnitude at 300 K is achieved. The electrical resistivity decrease is even higher if we considered that the resistivity of the undoped sample grown at pH 9.0 would have a higher resistivity than the sample shown in Fig. 8 and grown at pH 10.0.[56] This is a significant decrease in electrical resistivity by doping if we compare with results in the literature, for example, Cu_2O doped with Mn that presented a decrease in resistivity of a factor of three at ∼300 K.[31] The electrical resistivity reduction due to Bi doping could be assigned to the enhancement of V_{Cu} density induced by the incorporation of Bi^{3+} ions into the Cu_2O lattice. This statement agrees with the optical and structural results discussed earlier. Moreover, the lowest electrical resistivity was found for Cu_2O deposited at −0.375 V *vs* SCE, and for this deposition potential the highest E_d value was calculated. Such correlation between electrical resistivity and E_d leads to the conclusion that Cu_2O depositions at less negative potentials will result in higher V_{Cu} concentrations.

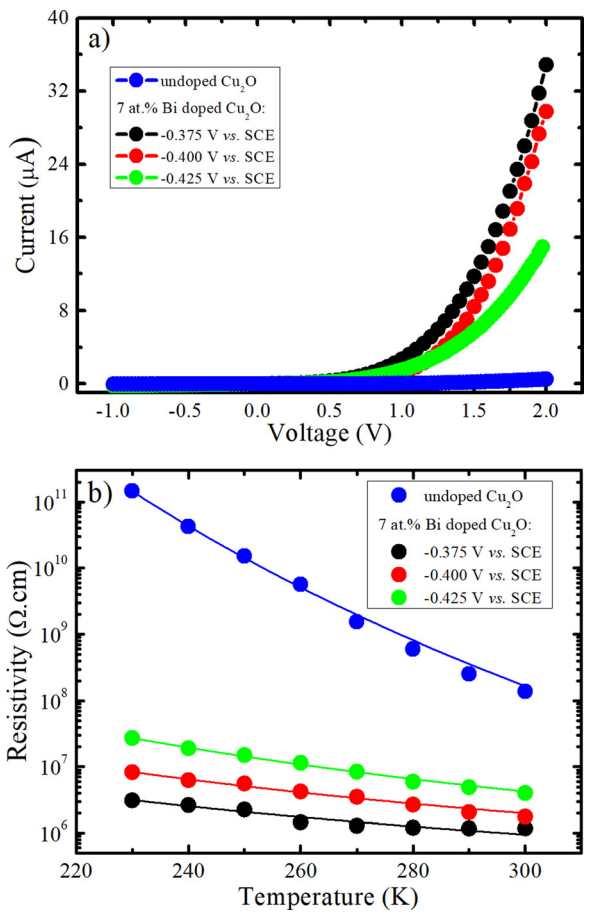

FIG. 8. (a) Current *vs*. voltage curves obtained at RT for undoped and Bi doped Cu_2O films. From the region at forward bias was calculated the resistivity for each sample. (b) Electrical resistivity as a function of temperature.

From the Arrhenius-like behavior of data in Fig. 8(b) was extracted the activation energy E_a. The value of 0.63 eV was found for undoped Cu_2O. This E_a agrees with the one theoretically calculated for acceptor levels arising from interstitial oxygen defects (O_i).[57] Photoinduced current transient spectroscopy experiments done by Rakhshani *et al.*[19] also displayed hole traps with an activation energy of 0.6 eV.

Among the Bi doped Cu_2O layers, E_a is equal to 0.17, 0.13 and 0.10 eV for electrodeposition potentials of −0.425, −0.400 and −0.375 V *vs*. SCE, respectively. In the literature, E_a for V_{Cu} has been calculated to be in the range of 0.10 to 0.28 eV (Refs. 2, 40, and 54), and experimentally, the range of 0.12 to 0.25 eV has been found.[19,58,59] As expected from E_d and electrical resistivity values, the concentration of V_{Cu} increases for less negative electrodeposition potentials. These findings allow us to suppose that under undoped conditions, O_i drives the Cu_2O electrical conduction, and when Bi^{3+} ions are incorporated into Cu_2O, the density of V_{Cu} becomes high enough to overcome the O_i contribution to the electrical transport.

D. First principles calculations

The structure of bismuth atoms in the Cu_2O host lattice was studied through computational simulation using DFT methods. Supercells containing different amounts of Bi, i.e., different concentrations of Bi, were relaxed until all the atoms reached a position in which the interacting forces between them are less than 0.01 eV/Å. Substitutional and interstitial conformations were considered; in either case, the addition of Bi atoms to the Cu_2O host induces a compressive stress. This occurs due to the larger ionic radius of Bi in comparison to Cu and O atoms, which makes the bond lengths around the dopant longer and pushes Cu and O atoms closer to each other. This stress can be compensated by an increase in the lattice parameter or by the introduction of vacancy defects.

Supercells containing different concentrations of substitutional Bi atoms (Bi_{Cu}), occupying Cu sites, were calculated in two configurations. One with Bi atoms occupies sites near each other, i.e., as close neighbors. Another configuration with Bi atoms is located in sites as far as possible, that is almost one lattice parameter for the case of a $2 \times 2 \times 2$ supercell. Figure 9(a) shows the relaxed structure of a host supercell, and in Figs. 9(b) and 9(c), supercells containing

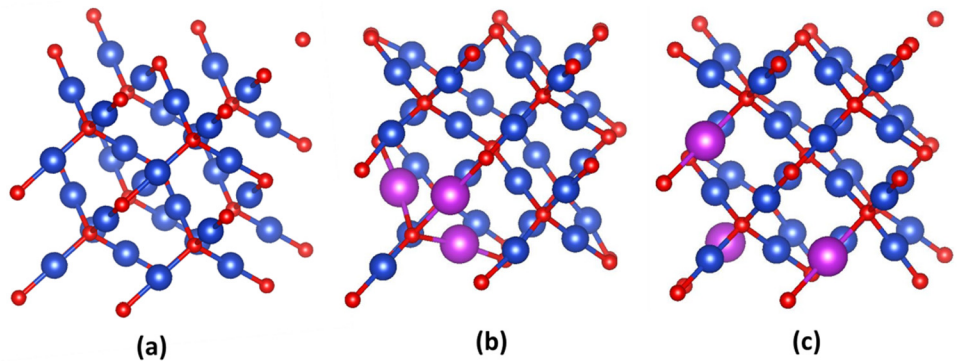

FIG. 9. (a) Relaxed structure of the Cu_2O host and (b) and (c) the relaxed structure of 6.2% Bi doped Cu_2O in near and far configurations, respectively. The atoms Cu, O and Bi are depicted in blue, red and magenta spheres, respectively.

3 atoms (6.2%) of Bi in close and far configurations, respectively. The far configuration of Bi atoms does not induce large distortions in the Cu_2O cell, except for an oxygen displacement generated by the Bi-O bond with a length of 2.347 Å, which is much larger than the usual Cu-O bond length of 1.856 Å in the host cell. In the case of the near configuration, substantial distortions are found due to the spherical expansion around the Bi atoms, decreasing the Bi-O bonds to 2.290 Å and decreasing the Cu-O bonds to 1.741 Å.

In Table II are shown the values of the heat of formation for supercells with different concentrations of Bi, in both near and far configurations. The data show that increasing the number of Bi up to 3, the heat of formation slightly raises about 0.3 eV for both cases, near and far. By inserting a fourth bismuth atom in the cell, it causes an increase in the heat of formation of about 0.25 eV in the near configuration and 0.75 eV in the far configuration. This indicates that the introduction of a higher amount of Bi beyond 6.2% is energetically unfavorable, meaning this value being a dilution limit for Bi in a Cu_2O host cell. It is a result that is consistent with the experimental findings of XRD and TEM, showing no evidence for Bi phases for concentrations of up to about 7 at. % of Bi Cu_2O layers. From the differences in the heat of formation in the near and far configurations shown in Table II, it is possible to infer that the near configuration of Bi atoms is the most stable one, for all concentrations treated here.

Figure 10 (a) presents the graph of formation energy *vs.* pH. The pH equilibrium conditions are generated by the equations given in Sec. II B and the formation energy is calculated with Eq. (1). Two types of interstitial dopants were calculated, one occupying an octahedral site ($I_{Bi\text{-}oct}$) and the other occupying a tetrahedral site ($I_{Bi\text{-}tet}$), both surrounded by copper atoms. In the whole range of pH, the formation energies of interstitial defects are much higher in comparison to substitutional Bi in Cu (Bi_{Cu}) sites. In a basic environment, V_{Cu} should be the most concentrated defects. Additionally, the formation energy for substituting Cu by Bi increases with the pH, making the doping process difficult at very high pH values.

Nonetheless, once Bi doping occurred, the formation energy needed to generate a copper vacancy in Cu_2O is reduced. Figure 10(b) shows the V_{Cu} formation energy in different Cu_2O supercells vs. pH. V_{Cu}^{Host} is the formation energy of a copper vacancy in undoped Cu_2O, while $V_{Cu}^{2\%Bi}$ ($V_{Cu}^{6\%Bi}$) is the formation energy of a vacancy in a 2% (6%) bismuth doped Cu_2O host, i.e., in a supercell with one (three) bismuth atoms in place of copper atoms. The $V_{Cu}^{2\%Bi}$ ($V_{Cu}^{6\%Bi}$) formation energy is calculated by subtracting the

TABLE II. The number of Bi atoms in the supercell, their respective concentrations, E is the heat of formation, E_{near} in the heat of formation in the near configuration and E_{far} in the heat of formation in the far configuration and ΔE is the difference in the heat of formation of near and far configurations (or clustering energy).

Number of Bi atoms	Concentration	E (eV)		
0	0	−1.529		
1	2.1	−1.424		
Number of Bi atoms	Concentration	E_{near} (eV)	E_{far} (eV)	$\Delta E = E_{near} - E_{far}$ (eV)
2	4.1	−1.343	−1.281	−0.062
3	6.2	−1.250	−1.190	−0.060
4	8.3	−1.002	−0.464	−0.538

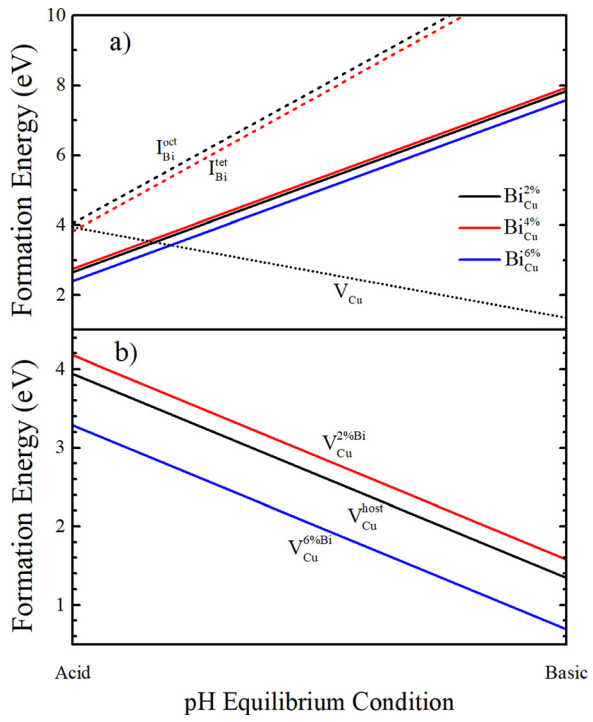

FIG. 10. Graph of formation energy vs. pH of growth medium; in (a), for different doping conformations and concentrations and in (b), the formation energy of a copper vacancy for host cells with different Bi concentrations.

formation energy of a supercell containing both one (three) Bi_{Cu} dopant(s) and one Cu vacancy by the formation energy of a supercell containing just one (three) Bi_{Cu}. The smaller formation energy of $V_{Cu}^{6\%Bi}$ in comparison to a simple V_{Cu}^{Host}, and even $V_{Cu}^{2\%Bi}$, indicates that once three copper sites are substituted by bismuth atoms, the introduction of a copper vacancy becomes more favorable. Thus, the number of vacancies should be enhanced by Bi doping, which corroborates with the experimental findings. The high stability of copper vacancies in Bi doped Cu_2O can be discussed in two terms, first due to structural relaxation, in which the stress induced by the large bismuth atom occupying a copper site is reduced by the removal of a neighboring copper creating a vacancy. Second, the high oxidation state of bismuth (+3) in comparison to copper (+2) decreases the Cu-O binding energy around the Bi dopant, making it easier to create a copper vacancy.

The electronic structure of Bi doped Cu_2O was calculated by using hybrid functionals and spin-orbit coupling; the energy bandgap and single particle levels (SPL) for each configuration were obtained. In Fig. 11(a) is presented a diagram showing the bandgap values and the SPL for some relevant doping situations. The bandgap for the host structure of Cu_2O is about 1.95 eV, very close to experimental values[17] and to other hybrid-DFT reported bandgap of 1.91 eV.[60] Before taking into account the spin-orbit coupling, the calculated band gap was 2.05 eV, indicating a small spin-orbit interaction. The introduction of a single V_{Cu} in the host supercell slightly increases the calculated bandgap; the dashed lines across Fig. 11(a) indicate the VBM and the conduction-band minimum (CBM) of the host supercell and the HOMO of the defective cell, which was aligned with the VBM of the host supercell. A relevant shift of the band gap to higher values (blue-shift) is only seen in the case of large amounts of Bi doping, i.e., about 6% bismuth in Cu_2O, reaching a value of 2.17 eV. These last results are for structures with Bi atoms in near configuration. This increase of the bandgap is consistent with experimental observations shown above, and is attributed to distortions in the crystal lattice driven by the large size of bismuth atoms since no traces of bismuth orbitals in the valence and conduction bands were seen in the density of states (results not shown).

The acceptor SPL induced inside of the band gap by a single V_{Cu} occurs at 0.61 eV above the VBM, close to 0.52 eV found for the same defect in Ref. 2 using the HSE (Heyd-Scuseria-Ernzerhof) functional and 0.45 eV found experimentally.[58] The introduction of a single Bi_{Cu} dopant creates a double degenerated acceptor level lying deep in the bandgap, 1.23 eV above the valence band, mainly due to the Bi *p*-orbital. Nonetheless, this level has not been found experimentally. The addition of V_{Cu} to the single doped supercell splits off the degenerated Bi_{Cu} SPL and induce an additional acceptor level at about 0.42 eV above the VBM. The latter acceptor level is also introduced when a vacancy is added to a 6% doped host cell ($3Bi_{Cu} + V_{Cu}$), but at 0.68 eV above the VBM.

To compare the DFT results to the electrical measurements, the transition levels for some defects were calculated. The transition levels were obtained by taking the SPL of a charged supercell after a proper relaxation. The results are presented in Fig. 11(b). After occupying the acceptor SPL of a simple V_{Cu}, the level becomes shallower, about 0.14 eV above the VBM, in agreement with the previous electrical characterization of Cu_2O.[19,59] Scanlon *et al.*[2] found a transition level at about 0.23 eV for a V_{Cu}. Transition energies at 0.06 eV and 0.19 eV were found for a copper vacancy in a 2% and 6% Bi doped Cu_2O host supercell, respectively.

In the electrical measurement, undoped samples presented an activation energy of about 0.6 eV, while by doping the value decreases to below 0.2 eV, reaching 0.1 eV for the sample grown at an electrodeposition potential of −0.375 V.

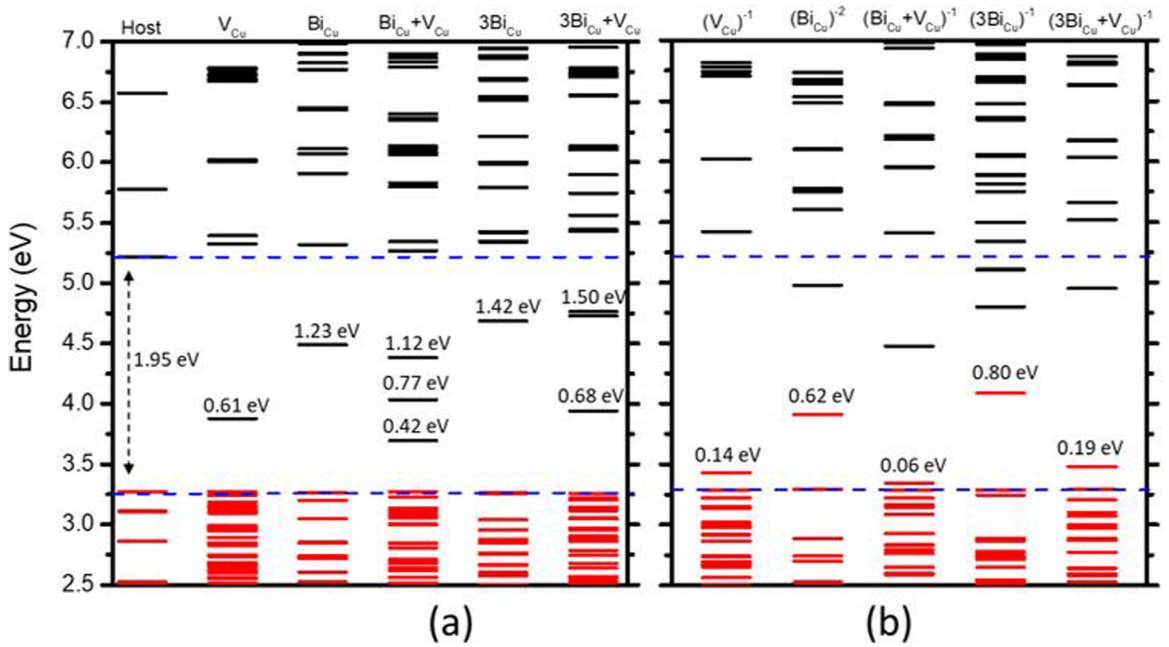

FIG. 11. Diagrams of the bandgap and the SPL in Cu_2O. (a) SPL for the calculated supercell with bismuth and copper vacancies in the neutral charge condition. (b) SPL for the same supercell in the charged condition.

An activation energy of around 0.6 eV above the VBM has been previously reported by Rakhshani[19] and Mahalingam[61] in electrodeposited samples, being attributed to hole traps. Theoretical results using the DFT methodology and the GGA functional point to the existence of acceptor levels due to an interstitial oxygen at about 0.6 eV above the VBM,[54] which could act as a hole trap. However, by using HSE functionals, the transition levels for interstitial oxygens only occur deep in the band gap, such as 1.25 eV found here and 1.08 eV found elsewhere.[2] Even through the theoretical transition energy for interstitial oxygens disagrees with experimental activation energies, such defects stand as the most probable source of deep acceptors in Cu_2O. Once doped with Bi, the measured activation energy becomes shallower, which can be correlated to copper vacancy induced acceptors levels. The results shown above point to the fact that Bi alone cannot generate levels around to the ones found experimentally. However, the level at 0.19 eV, found for a vacancy in a 6% Bi doped Cu_2O supercell is in the same order of the values found in the electrical transport experiments.

IV. CONCLUSIONS

In summary, we experimentally and theoretically investigated the Cu_2O doping by Bi atoms. We presented an electrochemical route that is able to produce 7 at. % Bi-doped Cu_2O films without secondary phases and with an electrical resistivity of at least two orders of magnitude lower than the one measured for undoped Cu_2O films. The lattice parameter and the optical properties as a function of Bi doping indicated an enhancement of the concentration of V_{Cu} defects in the Cu_2O films when they are Bi doped. This observation was supported by DFT calculations, which showed that V_{Cu} formation energy is smaller in cells containing 6% of Bi atoms in comparison to undoped host cells. Moreover, the measured activation energy for 7 at. % Bi doped Cu_2O films agrees well with the one calculated by DFT for V_{Cu} in a 6% Bi doped Cu_2O supercell. The enhancement of V_{Cu} concentration is probably the cause of the Cu_2O electrical resistivity decrease with Bi doping.

ACKNOWLEDGMENTS

We offer our thanks to the Brazilian agencies CNPQ, CAPES, FAPESC, and FINEP for providing additional support to this work. The authors also thank Professor D. F. Franceschini Filho from Instituto de Física, UFF, for XPS measurements and Professor J. F. Dias from Instituto de Física, UFRGS, for PIXE measurements. All the computational calculations were done in the CENAPAD-SP cluster at Campinas/SP.

[1]S. Nikitine, J. B. Grun, and M. Sieskind, J. Phys. Chem. Solids **17**, 292 (1961).
[2]D. Scanlon, B. Morgan, G. Watson, and A. Walsh, Phys. Rev. Lett. **103**, 96405 (2009).
[3]A. Paracchino, V. Laporte, K. Sivula, M. Grätzel, and E. Thimsen, Nat. Mater. **10**, 456 (2011).
[4]R. G. Delatorre, M. L. Munford, R. Zandonay, V. C. Zoldan, A. A. Pasa, W. Schwarzacher, M. S. Meruvia, and I. A. Hümmelgen, Appl. Phys. Lett. **88**, 233504 (2006).
[5]S. Song, R. Rao, H. Yang, and A. Zhang, J. Phys. Chem. C **114**, 13998 (2010).
[6]H. Huang, J. Zhang, L. Jiang, and Z. Zang, J. Alloys Compd. **718**, 112 (2017).
[7]A. Mittiga, E. Salza, F. Sarto, M. Tucci, and R. Vasanthi, Appl. Phys. Lett. **88**, 163502 (2006).
[8]J. Wei, Z. Zang, Y. Zhang, M. Wang, J. Du, and X. Tang, Opt. Lett. **42**, 911 (2017).
[9]A. Chen, H. Long, X. Li, Y. Li, G. Yang, and P. Lu, Vacuum **83**, 927 (2009).
[10]J. Deuermeier, J. Gassmann, J. Brötz, and A. Klein, J. Appl. Phys. **109**, 113704 (2011).
[11]Z. Zang, A. Nakamura, and J. Temmyo, Opt. Express **21**, 11448 (2013).
[12]T. D. Golden, M. G. Shumsky, Y. Zhou, R. A. VanderWerf, R. A. Van Leeuwen, and J. A. Switzer, Chem. Mater. **8**, 2499 (1996).
[13]I. S. Brandt, M. A. Tumelero, S. Pelegrini, G. Zangari, and A. A. Pasa, J. Solid State Electrochem. **21**, 1999 (2017).
[14]A. Kampmann, V. Sittinger, J. Rechid, and R. Reineke-Koch, Thin Solid Films **361**, 309 (2000).
[15]D. Lincot, J. F. Guillemoles, S. Taunier, D. Guimard, J. Sicx-Kurdi, A. Chaumont, O. Roussel, O. Ramdani, C. Hubert, J. P. Fauvarque, N. Bodereau, L. Parissi, P. Panheleux, P. Fanouillere, N. Naghavi, P. P. Grand, M. Benfarah, P. Mogensen, and O. Kerrec, Sol. Energy **77**, 725 (2004).
[16]J. N. Yao, P. Chen, and A. Fujishima, J. Electroanal. Chem. **406**, 223 (1996).
[17]I. S. Brandt, C. A. Martins, V. C. Zoldan, A. D. C. Viegas, J. H. D. da Silva, and A. A. Pasa, Thin Solid Films **562**, 144 (2014).
[18]A. E. Rakhshani, J. Appl. Phys. **69**, 2365 (1991).
[19]A. E. Rakhshani, Y. Makdisi, and X. Mathew, Thin Solid Films **288**, 69 (1996).
[20]I. S. Brandt, C. I. L. de Araujo, V. Stenger, R. G. Delatorre, and A. A. Pasa, ECS Trans. **14**, 413 (2008).
[21]K. Han and M. Tao, Sol. Energy Mater. Sol. Cells **93**, 153 (2009).
[22]I. S. Brandt, M. A. Tumelero, E. Lima, Jr., D. L. da Silva, R. D. Zysler, R. Faccio, and A. A. Pasa, J. Magn. Magn. Mater. **441**, 374 (2017).
[23]K. D. Schroder, *Semiconductor Material and Device Characterization* (John Wiley & Sons, Inc., Hoboken, 2005).
[24]H. M. Wei, H. B. Gong, L. Chen, M. Zi, and B. Q. Cao, J. Phys. Chem. C **116**, 10510–10515 (2012).
[25]C. M. McShane and K.-S. Choi, Phys. Chem. Chem. Phys. **14**, 6112 (2012).
[26]C. M. McShane, W. P. Siripala, and K.-S. Choi, J. Phys. Chem. Lett. **1**, 2666 (2010).
[27]R. P. Wijesundera, L. K. A. D. D. S. Gunawardhana, and W. Siripala, Sol. Energy Mater. Sol. Cells **157**, 881 (2016).
[28]S. Fanssila, *Introduction to Microfabrication* (John Wiley & Sons Ltd., Chichester, 2004).
[29]X. Han, K. Han, and M. Tao, Electrochem. Solid-State Lett. **12**, H89 (2009).
[30]S. Pelegrini, C. I. L. de Araujo, R. C. da Silva, A. D. C. Viegas, and A. A. Pasa, ECS Trans. **31**, 143 (2010).
[31]Y. L. Liu, S. Harrington, K. A. Yates, M. Wei, M. G. Blamire, J. L. MacManus-Driscoll, and Y. C. Liu, Appl. Phys. Lett. **87**, 222108 (2005).
[32]S. Ishizuka, S. Kato, Y. Okamoto, and K. Akimoto, Appl. Phys. Lett. **80**, 950 (2002).
[33]S. Ishizuka and K. Akimoto, Appl. Phys. Lett. **85**, 4920 (2004).
[34]Y. S. Lee, J. Heo, M. T. Winkler, S. C. Siah, S. B. Kim, R. G. Gordon, and T. Buonassisi, J. Mater. Chem. A **1**, 15416 (2013).
[35]Z. Zang, A. Nakamura, and J. Temmyo, Mater. Lett. **92**, 188 (2013).
[36]G. Kresse and J. Furthmüller, Phys. Rev. B **54**, 11169 (1996).
[37]J. P. Perdew, K. Burke, and M. Ernzerhof, Phys. Rev. Lett. **77**, 3865 (1996).
[38]J. Heyd, G. E. Scuseria, and M. Ernzerhof, J. Chem. Phys. **118**, 8207 (2003).
[39]P. E. Blöchl, Phys. Rev. B **50**, 17953 (1994).
[40]D. O. Scanlon, B. J. Morgan, and G. W. Watson, J. Chem. Phys. **131**, 124703 (2009).
[41]W. Wang, D. Wu, Q. Zhang, L. Wang, and M. Tao, J. Appl. Phys. **107**, 123717 (2010).
[42]W. E. Morgan, W. J. Stec, and J. R. Van Wazer, Inorg. Chem. **12**, 953 (1973).
[43]Inorganic Crystal Structure Database (ICSD), Fachinformationszentrum Karlsruhe, Germany and the U.S. Department of Commerce on Behalf of the United States (2007).

[44]M. Nolan and S. D. Elliott, Chem. Mater. **20**, 5522 (2008).
[45]J. A. Switzer, H. M. Kothari, and E. W. Bohannan, J. Phys. Chem. B **106**, 4027 (2002).
[46]I. S. Brandt, V. C. Zoldan, V. Stenger, C. C. Plá Cid, A. A. Pasa, T. J. Oliveira, and F. D. A. Aarão Reis, J. Appl. Phys. **118**, 145303 (2015).
[47]J. A. Switzer, R. Liu, E. W. Bohannan, and F. Ernst, J. Phys. Chem. B **106**, 12369 (2002).
[48]S. Fletcher, J. Electroanal. Chem. **118**, 419 (1981).
[49]A. Buljan, M. Llunell, E. Ruiz, and P. Alemany, Chem. Matter **13**, 338 (2001).
[50]A. Filippetti and V. Fiorentini, Phys. Rev. B **72**, 35128 (2005).
[51]S. H. Wemple and M. DiDomenico, Jr., Phys. Rev. B **3**, 1338 (1971).
[52]A. L. J. Pereira and J. H. D. da Silva, J. Non-Cryst. Solids **354**, 5372 (2008).
[53]S. Pelegrini, M. A. Tumelero, I. S. Brandt, R. D. Della Pace, R. Faccio, and A. A. Pasa, J. Appl. Phys. **123**, 161567 (2018).
[54]H. Raebiger, S. Lany, and A. Zunger, Phys. Rev. B **76**, 45209 (2007).
[55]S. K. Cheung and N. W. Cheung, Appl. Phys. Lett. **49**, 85 (1986).
[56]During current *vs*. voltage measurements of undoped samples (deposited at pH 9.0) two types of electrical behaviors were observed. One totally insulating, with no current flowing through the thin film even for high electrical applied potential, and another very conductive with calculated resistivity comparable with the n-Si(100) one. The first behavior is explained by the high resistivity of the Cu_2O thin film deposited at pH 9.0. It is expected an electrical resistivity enhancement of at least 2 orders of magnitude by reducing the pH from 10.0 to 9.0, as found in Ref. 21, and this increase can put the resistance of our samples outside equipment's work range. The second behavior is attributed to pinholes or copper filaments, which strongly reduce the resistance of the system.
[57]A. Soon, X.-Y. Cui, B. Delley, S.-H. Wei, and C. Stampfl, Phys. Rev. B **79**, 35205 (2009).
[58]G. K. Paul, Y. Nawa, H. Sato, T. Sakurai, and K. Akimoto, Appl. Phys. Lett. **88**, 141901 (2006).
[59]G. K. Paul, R. Ghosh, S. K. Bera, S. Bandyopadhyay, T. Sakurai, and K. Akimoto, Chem. Phys. Lett. **463**, 117 (2008).
[60]Q. Bai, W. Wang, Q. Zhang, and M. Tao, J. Appl. Phys. **111**, 23709 (2012).
[61]T. Mahalingam, J. S. P. Chitra, S. Rajendran, and P. J. Sebastian, Semicond. Sci. Technol. **17**, 565 (2002).